The Astrophysical Journal Letters, 940:L13 (7pp), 2022 November 20 https://doi.org/10.3847/2041-8213/aca075

Reconciling Parker Solar Probe Observations and Magnetohydrodynamic Theory

Tommaso Alberti[1], Simone Benella[1], Giuseppe Consolini[1], Mirko Stumpo[1,2], and Roberto Benzi[2]
[1] INAF-Istituto di Astrofisica e Planetologia Spaziali, I-00133 Roma, Italy; tommaso.alberti@inaf.it
[2] Università degli Studi di Roma Tor Vergata, Dipartimento di Fisica, I-00133 Roma, Italy
Received 2022 September 22; revised 2022 October 27; accepted 2022 October 28; published 2022 November 17

Abstract

The Parker Solar Probe mission provides a unique opportunity to characterize several features of the solar wind at different heliocentric distances. Recent findings have shown a transition in the inertial range spectral and scaling properties around 0.4–0.5 au when moving away from the Sun. Here we provide, for the first time, how to reconcile these observational results on the radial evolution of the magnetic and velocity field fluctuations with two scenarios drawn from the magnetohydrodynamic theory. The observed breakdown is the result of the radial evolution of magnetic field fluctuations and plasma thermal expansion affecting the distribution between magnetic and velocity fluctuations. The two scenarios point toward an evolving nature of the coupling between fields that can be also reconciled with Kraichnan and Kolmogorov pictures of turbulence. Our findings have important implications for turbulence studies and modeling approaches.

Unified Astronomy Thesaurus concepts: Solar wind (1534); Interplanetary turbulence (830); Magnetohydrodynamics (1964); Interplanetary magnetic fields (824)

1. Introduction

Since 2018 the Parker Solar Probe (PSP) mission is collecting solar wind plasma and magnetic field data through the inner heliosphere, reaching the closest distance to the Sun ever reached by any previous mission (Fox et al. 2016; Kasper et al. 2021). Thanks to the PSP journey around the Sun (it has completed 11 orbits) a different picture has been drawn for the near-Sun solar wind with respect to the near-Earth one (Bale et al. 2019; Kasper et al. 2019; Chhiber et al. 2020; Malaspina et al. 2020; Bandyopadhyay et al. 2022; Zank et al. 2022). Different near-Sun phenomena have been frequently encountered, with the emergence of magnetic field flips, i.e., the so-called switchbacks (Dudok de Wit et al. 2020; Zank et al. 2020), kinetic-scale current sheets (Lotekar et al. 2022), and a scale-invariant population of current sheets between ion and electron inertial scales (Chhiber et al. 2021). Going away from the Sun (from 0.17 to 0.8 au), evidence of radial evolution of different properties of solar wind turbulence (Chen et al. 2020) as the spectral slope of the inertial range (from $-3/2$ close to the Sun to $-5/3$, at distances larger than 0.4 au), an increase of the outer scale of turbulence, a decrease of the Alfvénic flux, and a decrease of the imbalance between outward (z^+) and inward (z^-) propagating components (Chen et al. 2020) has been provided. Although the near-Sun solar wind shares different properties with the near-Earth one (Allen et al. 2020; Cuesta et al. 2022), significant differences have been also found in the variance of magnetic fluctuations (about 2 orders of magnitude) and in the compressive component of inertial range turbulence. In a similar way, Alberti et al. (2020) first reported a breakdown of the scaling properties of the energy transfer rate, likely related to the breaking of the phase-coherence of inertial range fluctuations. These findings, also highlighted by Telloni et al. (2021) and Alberti et al. (2022) analyzing a radial alignment between PSP and Solar Orbiter, and PSP and BepiColombo, respectively, have been interpreted as an increase in the efficiency of the nonlinear energy cascade mechanism when moving away from the Sun. More recently, by investigating the helical content of turbulence Alberti et al. (2022) highlighted a damping of magnetic helicity over the inertial range between 0.17 and 0.6 au suggesting that the solar wind develops into turbulence by a concurrent effect of large-scale convection of helicity and creation/annihilation of helical wave structures. All these features shed new light onto the radial evolution of solar wind turbulence that urges to be considered in expanding models of the solar wind (Verdini et al. 2019; Grappin et al. 2021), and also to reproduce and investigate the role of proton heating and anisotropy of magnetic field fluctuations (Hellinger et al. 2015).

First attempts to connect observational results obtained by PSP and theoretical predictions have been mainly devoted to turbulence transport models in a nearly incompressible magnetohydrodynamic (NI MHD) framework (Zank et al. 2017). As an example, Adhikari et al. (2020) reported on a plausible agreement between the radial evolution of some turbulent quantities (e.g., the fluctuating kinetic energy, the correlation length) derived from PSP's first orbit (between 0.17 and 0.61 au) and numerical solutions of the NI MHD turbulence transport model (Zank et al. 2017). Thus, the NI MHD model has been used to derive additional turbulent quantities such as the cascade rate, the ratio between the variance of inward (z^-) and outward (z^+) modes, the anisotropy in the energy-containing range, the role of the quasi-two-dimensional and the slab components of turbulence, the normalized cross-helicity σ_C, and the residual energy σ_R (e.g., Adhikari et al. 2020). In agreement with previous theoretical expectations (Adhikari et al. 2015; Zank et al. 2017, 2018) they found that σ_R decreases with increasing distance from the Sun, in agreement with a reasonable correlation between the most Alfvénic events ($\sigma_C \to 1$) and both increases in the energy cascade rate and local temperature (Andrés et al. 2022). These recent observations and theoretical findings suggest revising an old view by Dobrowolny et al. (1980) according to which an initially asymmetric MHD

turbulence, as that observed by PSP close to the Sun with an abundance of outward-propagating modes z^+, in absence of nonlinear interactions, relaxes toward a state characterized by the absence of one of the possible modes z^+ or z^-. That is, what is the role of nonlinear interactions in generating inward-propagating (z^-) modes such as those at larger distances from the Sun that we can observe?

In this work we start with the same theoretical framework of the NI MHD proposed by Zank et al. (2017) but we focus our attention on the consequences of observing an imbalanced turbulence close to the Sun, with $z^+ \gg z^-$, evolving toward a more balanced state with the radial distance, with $z^+ \sim z^-$. We find evidence of two different scenarios: Alfvénically dominated up to 0.3 au and magnetically dominated at larger distances (greater than 0.6 au). The observed breakdown is the result of the radial evolution of the distribution between magnetic and velocity fluctuations and their mutual coupling. The two scenarios can be also reconciled with Kraichnan and Kolmogorov pictures of turbulence in terms of the radial evolution of the coupling between fields. The manuscript is organized as follows: Section 2 introduces the theoretical framework, while Section 3 presents the observational results; finally, Section 4 summarizes the results and provides the outlook for future investigations.

2. Theoretical Background

As in Zank et al. (2017) we use the incompressible ($\nabla \cdot \boldsymbol{z}^{\pm} = 0$) MHD equations

$$\partial_t \boldsymbol{z}^{\pm} + (\boldsymbol{C_A} \cdot \nabla)\boldsymbol{z}^{\pm} + (\boldsymbol{z}^{\mp} \cdot \nabla)\boldsymbol{z}^{\pm} = -\frac{1}{\rho_0}\nabla p + \nu^{\pm}\nabla^2 \boldsymbol{z}^{\pm}, \tag{1}$$

where $\boldsymbol{z}^{\pm} = \boldsymbol{v} \pm \boldsymbol{b}$ are the Elsässer variables (Elsasser 1950), $\boldsymbol{v}$ being the fluctuating velocity field, and $\boldsymbol{b} = \frac{\boldsymbol{B}}{\sqrt{\mu_0 \rho_0}}$ being the fluctuating magnetic field in Alfvén units, $C_{\rm A} = \frac{B_0}{\sqrt{\mu_0 \rho_0}}$ being the background Alfvén speed, ρ_0 being the mass density, p being the kinetic pressure, and $\nu^{\pm}$ being the dissipative coefficients. The Elsässer variables describe the inward- and outward-propagating modes (Elsasser 1950).

As first noted by Chen et al. (2020) with PSP measurements outward-propagating modes z^+ have a stronger radial dependence with respect to inward modes z^- ($z^+ \sim r^{-0.85}$ versus $z^- \sim r^{-0.25}$), traducing into a radial trend of their ratio

$$R^{\pm} = \frac{z^+}{z^-} \sim r^{-0.6}. \tag{2}$$

This means that moving from 1 to 0.1 au the ratio increases by a factor of 4, although $z^{\pm}$ show a similar spectral exponent at variance of the heliocentric distance (Chen et al. 2020). Thus, close to the Sun we are in an unbalanced scenario in which $|z^+| \gg |z^-|$, evolving toward a balanced one $|z^+| \sim |z^-|$, typically observed at distances larger than 0.5–0.6 au (Chen et al. 2020). Furthermore, inward-propagating modes have a longer correlation time than outward ones (Chen et al. 2020; Cuesta et al. 2022), thus strengthening the hypothesis that z^- modes are generated via the reflection of z^+ ones, i.e., the nonlinear term is responsible for the observed radial trend (Matthaeus et al. 1994; Adhikari et al. 2015). This suggests investigating more deeply into what the consequences are of Equation (2). Indeed, the existence of two states, i.e., $|z^+| \gg |z^-|$ close to the Sun and $|z^+| \sim |z^-|$ at larger distances, can be traduced into a different nature of the coupling between $\boldsymbol{v}$ and $\boldsymbol{b}$ as follows.

The condition $|z^+| \sim |z^-|$ means

$$|\boldsymbol{v} + \boldsymbol{b}| \sim |\boldsymbol{v} - \boldsymbol{b}| \tag{3}$$

or equivalently

$$|\boldsymbol{v}|^2 + |\boldsymbol{b}|^2 + 2\boldsymbol{v} \cdot \boldsymbol{b} \sim |\boldsymbol{v}|^2 + |\boldsymbol{b}|^2 - 2\boldsymbol{v} \cdot \boldsymbol{b} \tag{4}$$

that is

$$\boldsymbol{v} \cdot \boldsymbol{b} \sim 0. \tag{5}$$

Thus, $|z^+| \sim |z^-|$ traduces into $\boldsymbol{v} \perp \boldsymbol{b}$.

Conversely, the condition $|z^+| \gg |z^-|$ is

$$|\boldsymbol{v} + \boldsymbol{b}| \gg |\boldsymbol{v} - \boldsymbol{b}| \tag{6}$$

that corresponds to

$$|\boldsymbol{v}|^2 + |\boldsymbol{b}|^2 + 2\boldsymbol{v} \cdot \boldsymbol{b} \gg |\boldsymbol{v}|^2 + |\boldsymbol{b}|^2 - 2\boldsymbol{v} \cdot \boldsymbol{b}, \tag{7}$$

and leading to

$$\boldsymbol{v} \cdot \boldsymbol{b} \gg 0. \tag{8}$$

This condition is, in principle, satisfied for any angle between the two fields $\theta_{vb} \neq 90°$, being maximized for the case $\boldsymbol{v} \| \boldsymbol{b}$; the latter satisfied under specific geometrical constraints and/or physical conditions. Thus, by neglecting the nonlinear term in Equation (1) and by considering PSP observations as a function of the heliocentric distance the relaxation from an initially asymmetric state ($|z^+| \gg |z^-|$) toward a symmetric one ($|z^+| \sim |z^-|$) supports the existence of a different degree of correlation between the fluctuating magnetic and velocity fields. This reflects into a different distribution of the value of the angle θ_{vb}, thus claiming a closed link between the variance/correlation anisotropy and the nature of MHD turbulence (Adhikari et al. 2022).

As usual in MHD turbulence (Matthaeus & Goldstein 1982; Roberts et al. 1987; Bavassano et al. 1998), two measurable quantities can be introduced to take into account the different role of magnetic and kinetic energies as well as the relations between fields fluctuations. These two parameters are the normalized cross-helicity σ_C and the normalized residual energy σ_R

$$\sigma_C = \frac{2\langle \boldsymbol{v} \cdot \boldsymbol{b} \rangle}{\langle \boldsymbol{v}^2 \rangle + \langle \boldsymbol{b}^2 \rangle} = \frac{\langle (z^+)^2 \rangle - \langle (z^-)^2 \rangle}{\langle (z^+)^2 \rangle + \langle (z^-)^2 \rangle}, \tag{9}$$

$$\sigma_R = \frac{\langle \boldsymbol{v}^2 \rangle - \langle \boldsymbol{b}^2 \rangle}{\langle \boldsymbol{v}^2 \rangle + \langle \boldsymbol{b}^2 \rangle} = \frac{R_{\rm A} - 1}{R_{\rm A} + 1}, \tag{10}$$

with $R_{\rm A} = \langle \boldsymbol{v}^2 \rangle / \langle \boldsymbol{b}^2 \rangle$ being the Alfvén ratio and $\langle \cdots \rangle$ stands for the time average; σ_C is a measure of the energy balance between outward- and inward-propagating fluctuations, while σ_R measures the balance between kinetic and magnetic energy; $\sigma_C = \pm 1$ evidences the presence of only one component (+: outward, −: inward), $|\sigma_C| < 1$ corresponds to the presence of both components and/or to non-Alfvénic fluctuations, while $\sigma_R = \pm 1$ evidences the existence of velocity-/magnetic-only fluctuations, with $\sigma_R = 0$ meaning equipartition.

The two scenarios drawn above immediately give us

$$|z^+| \sim |z^-| \Rightarrow \boldsymbol{v} \cdot \boldsymbol{b} = 0 \Rightarrow \sigma_C = 0, \tag{11}$$

$$|z^+| \gg |z^-| \Rightarrow \boldsymbol{v} \cdot \boldsymbol{b} \gg 0 \Rightarrow \sigma_C = 1. \tag{12}$$

Equations (11)–(12) clearly suggest that the two scenarios can be characterized via σ_C, with clear boundary values and varying between zero and one, while σ_R cannot be unambiguously determined. The observed scenarios drawn in terms of the normalized cross-helicity σ_C are in agreement with previous models, as the NI MHD model by Zank et al. (2017) predicting values larger than 0 within 1 au. In the following we explore our theoretical expectations by using PSP measurements in the inner heliosphere to compute the radial scaling of σ_C and σ_R as well as the joint probability of occurrence between pairs of values at different heliocentric distances. To compute σ_C and σ_R we use prescriptions that are widely adopted in the literature (e.g., Bavassano et al. 1998; D'Amicis & Bruno 2015). The polarity of $z^{\pm}$ modes is selected to always satisfy the condition that z^+ is an outward-propagating fluctuation in the solar wind reference frame as seen from the Sun. Then, $\sigma_{C,R}$ are computed using running averages over a window of 1 hr length shifted by 1 minute along the full data set. This procedure, although not preserving the independence of subsamples (as in Bavassano et al. 1998), allows us to increase the statistics. We have also verified that this preserves the significance of the results as also previously highlighted by Bruno et al. (2007) using Helios 2 data.

3. Parker Solar Probe Observations

We use PSP magnetic field and plasma measurements in the time interval from 2020 March 1 to 2022 March 1, i.e., covering seven PSP perihelia corresponding to encounters 5–11[3], although, as shown in Figure 1, the great majority of points (∼82%) belong to encounters 5–7 and encounter 11. However, our analysis is not focused on comparing different encounters but on a statistical analysis at different heliocentric distances. Thus, gaps in the data of a specific encounter do not affect our results. In detail, we used magnetic field data taken from the outboard fluxgate magnetometer from the FIELDS instrument suite (Bale et al. 2016) and are L2 quality data at 1 minute time resolution, while plasma measurements are obtained by the Solar Probe Cup of the SWEAP instrument suite (Kasper et al. 2016) and correspond to L3 quality data at 27.96 s time resolution. For our analysis, all data have been resampled at 1 minute resolution for consistency, forming a data set of $N = 1{,}051{,}200$ data points and covering the heliocentric range of distances between ∼0.1 and ∼0.85 au. However, the calibrated data points (*good quality* to be used in the analysis) are $N_{\rm cal} = 159{,}375$, corresponding to roughly 15% of the full data points. Figure 1 reports the plasma bulk speed V, the Alfvén speed $V_{\rm A} = 21.8\,\frac{B}{\sqrt{n}}$ (B in units of nT, n in units of cm^{-3}), and the PSP radial distance (in astronomical units) to the Sun R, respectively.

While a clear trend with the heliocentric distance R cannot be recovered for the plasma bulk speed (as expected), a dependence on R of the Alfvén speed $V_{\rm A}$ seems to be present, increasing as the Sun is approached (again, as expected). This suggests that the Alfvén field radially evolves according to both the large-scale configuration of the Parker spiral and the expansion of the solar wind plasma through the innermost heliosphere as an outward-streaming gas (Parker 1958).

[3] https://sppgway.jhuapl.edu/encounters

The first step of our analysis is to characterize the radial behavior of the reduced cross-helicity σ_C (blue) and the residual energy σ_R (red) as reported in Figure 2.

A clear radial dependence of the normalized cross-helicity σ_C is observed, while the residual energy σ_R is almost constant and always negative. Our results are consistent with those recently reported by Andrés et al. (2022) who found a nearly constant and negative σ_R at all heliocentric distances and an increasing σ_C with increasing temperature (i.e., decreasing distance). Furthermore, our results are qualitatively in agreement with Adhikari et al. (2020) and Zank et al. (2021) using the NI MHD model who reported a decreasing σ_C with increasing R, although disagreeing with the predicted behavior of σ_R (increasingly negative as R increases, Adhikari et al. 2020). Our results, thus, indicate a turbulent nature with prevailing 2D structures over the slab component (Oughton et al. 2016) as R increases. This behavior can be linked with the geometry between the large-scale solar wind speed and the magnetic field. Indeed, as recently shown by Adhikari et al. (2022) PSP only measures slab components close to the Sun since the flow is almost radial; conversely, as R increases the flow is not radial and then a predominance of the 2D component over the slab one is observed. Furthermore, our findings are in agreement with the two scenarios drawn in Section 2 in terms of σ_C, summarized in Equations (11)–(12), suggesting $\sigma_C \to 1$ close to the Sun (more precisely this condition is matched at the Alfvén point where $z^- = 0$ being $v = b$, e.g., Adhikari et al. 2019) and $\sigma_C \to 0$ far away.

To further exploit the nature of these two scenarios we evaluate the joint distribution of the values of the cross-helicity σ_C and the residual energy σ_R within two different bands of heliocentric distances: close to the Sun ($R \in [0.1, 0.3]$ au) and far away ($R \in [0.6–0.8]$ au). The choice of these two heliocentric ranges is consistent with previous observations reporting a different nature of the turbulent properties, changing around 0.4–0.5 au (Alberti et al. 2020; Chen et al. 2020; Stumpo et al. 2021). The results are shown in Figure 3.

Moving away from the Sun the distribution of pairs of (σ_C, σ_R) evolve from the fourth quadrant ($\sigma_C > 0$, $\sigma_R < 0$) at 0.1–0.3 au toward the third one ($\sigma_C < 0$, $\sigma_R < 0$) at 0.6–0.8 au. On one side, the decreases in the cross-helicity σ_C suggests an evolution from a more to a less Alfvénic turbulence, while the observed trend for the residual energy σ_R suggests a turbulence always with an excess of magnetic energy. Furthermore, although the predominant modes are always outward-propagating fluctuations (z^+), the presence of a nonnull probability of observing $\sigma_C < 0$ at 0.6–0.8 au implies an increase in the occurrence of inward fluctuations ($\sigma_C < 0$). The most interesting observation is that, while close to the Sun there is the possibility of observing only outward-propagating modes ($\sigma_C = 1$), this is forbidden at larger distances for both types of fluctuations (i.e., $\sigma_C \neq \pm 1$). This suggests that as we move away from the Sun the nonlinear term is becoming relevant, being able to generate inward-propagating modes. Interestingly, this is almost independent on σ_R, i.e., in terms of energy of fluctuations there is no evidence of a dynamical transition from magnetic to kinetic. We return to this point in Section 4. Thus, our findings are in agreement with the simple theoretical framework introduced in Equations (11)–(12), as well as with recently published literature (Andrés et al. 2022; Sioulas et al. 2022), and can be summarized as follows:

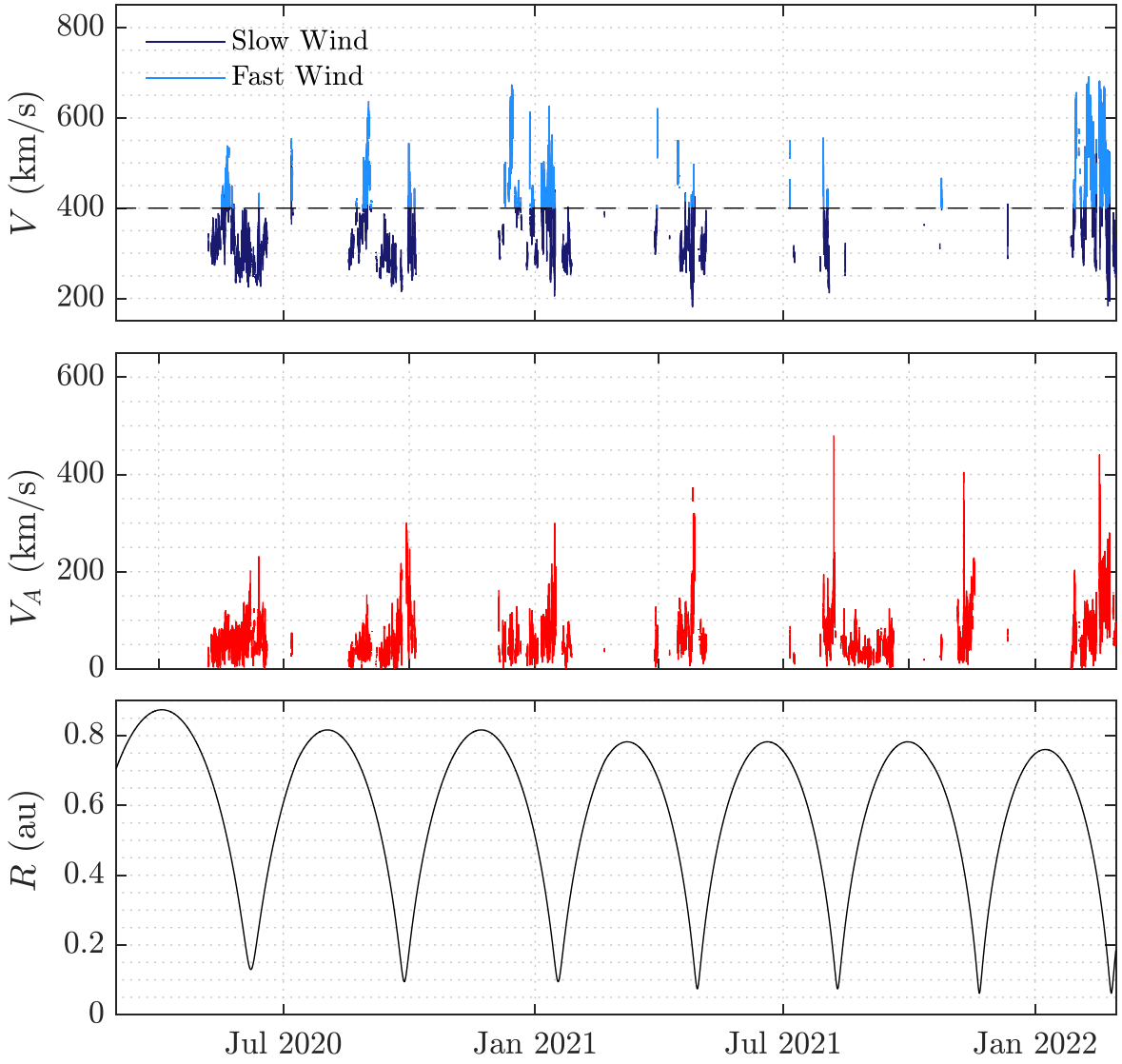

Figure 1. (From top to bottom) The plasma bulk speed V, the Alfvén speed $V_A = 21.8 \frac{B}{\sqrt{n}}$ (B in units of nT, n in units of cm^{-3}), and the PSP radial distance to the Sun R. Dark and light blue lines in the top panel refer to slow ($V < 400$ km s^{-1}) and fast ($V > 400$ km s^{-1}) solar wind intervals, respectively.

(i) $R \lesssim 0.3$ au: we observe the presence of a population of outward Alfvénic fluctuations with equiparted energy ($\sigma_C = 1$, $\sigma_R = 0$) and a population of non-Alfvénic fluctuations with an excess of magnetic energy ($\sigma_C \in [0, 1)$, $\sigma_R < 0$);

(ii) $R > 0.6$ au: we observe the presence of non-Alfvénic fluctuations or both outward and inward modes with an excess of magnetic energy ($\sigma_R < 0$). Note that in this range of heliocentric distances the existence of only inward/outward modes is forbidden (i.e., $\sigma_C \neq \pm 1$).

As a final step of our analysis, since the cross-helicity σ_C also depends on the solar wind speed, we investigated the joint distribution of pairs (σ_C, σ_R) within the same two heliocentric ranges ($R \in [0.1, 0.3]$ au and $R \in [0.6–0.8]$ au) by separating slow ($V < 400$ km s^{-1}) and fast ($V > 400$ km s^{-1}) solar wind intervals (Figure 1, top panel). The results are reported in Figure 4.

The results look interesting since we can highlight a clear different role in terms of solar wind streams. In particular, we observe a trend from (σ_C, σ_R) = (1, 0) to $\sigma_R < 0$ for the fast solar wind and a radial decreasing in terms of σ_R for the slow solar wind. The observed behavior of σ_C is again in agreement with our theoretical predictions, i.e., Equations (11)–(12), but also with previous models as the NI MHD one (Zank et al. 2017; Adhikari et al. 2020) and/or energy transfer rate estimations (Andrés et al. 2022). Furthermore, differently from the overall features of the solar wind (see Figure 2), i.e., when considering together fast and slow streams, the observed decreasing σ_R with increasing R for the slow solar wind is in agreement with the NI MHD model (Adhikari et al. 2020). This suggests that the NI MHD model can be particularly useful for investigating the radial evolution of solar wind turbulent quantities for slow solar wind streams. Thus, the energy-containing range for the slow solar wind can be described as a superposition of a (predominant) 2D component and a (less dominant) slab one (Zank et al. 2021), matching our findings when separating fast and slow winds.

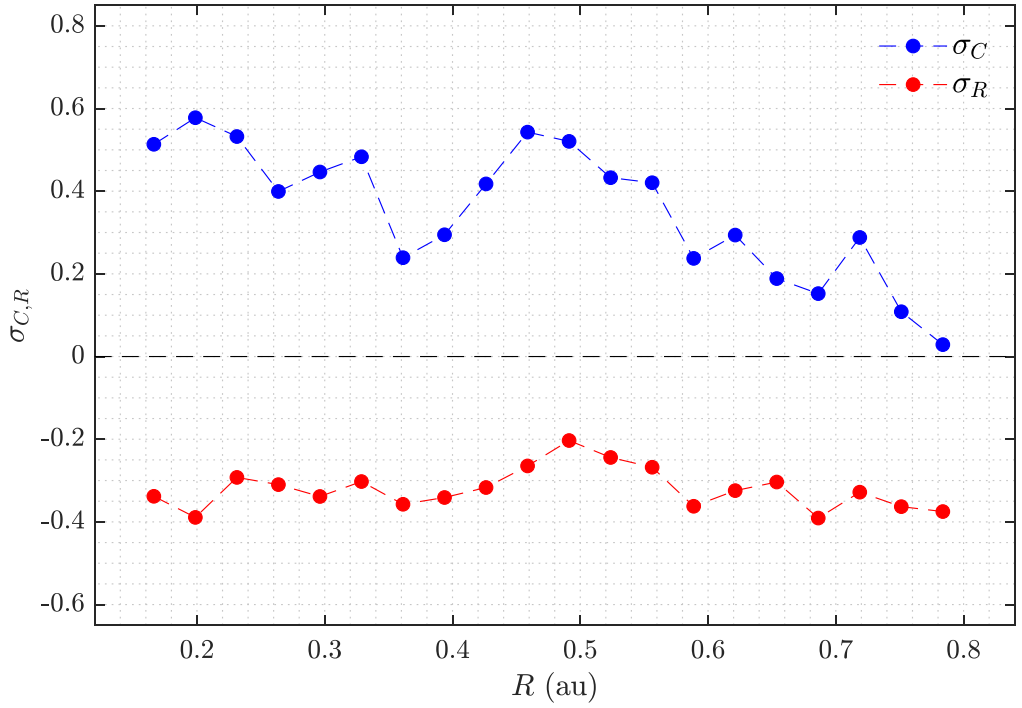

Figure 2. The radial dependence of the reduced cross-helicity σ_C (blue) and the residual energy σ_R (red).

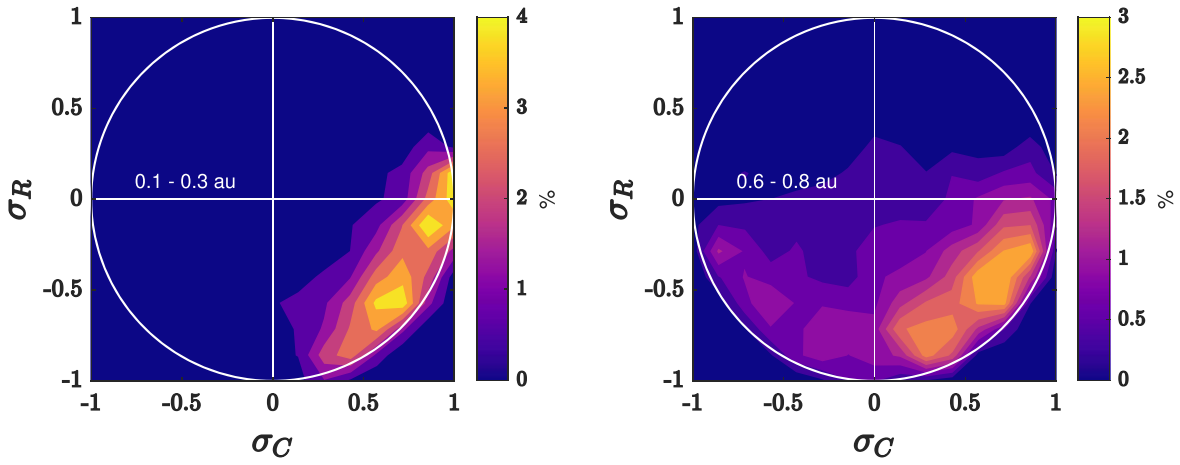

Figure 3. The joint distribution of the values of the normalized cross-helicity σ_C and the normalized residual energy σ_R within two heliocentric ranges: close to the Sun ($R \in [0.1, 0.3]$ au) and far away ($R \in [0.6–0.8]$ au). The color bar is the percentage ratio between the counts in each bin and the total number of calibrated (good quality) data points.

4. Conclusions

As a final task we discuss implications of our findings, trying to interpret them in the framework of turbulence. Earlier studies (e.g., Alberti et al. 2020; Chen et al. 2020) using PSP observations have shown that an MHD Alfvénic scenario is reached when approaching the Sun for the spectral and the scaling properties of the Elsässer field fluctuations, although mainly dominated by one mode (specifically, z^+), as well as for both the magnetic and the velocity field fluctuations across the inertial range, with a spectral exponent close to $-3/2$ (Chen et al. 2020). Conversely, at distances larger than 0.6 au all fields are characterized by a spectral exponent close to $-5/3$ (Chen et al. 2020), and both modes are almost equipartitioned ($|z^+|/|z^-| \sim 1$). According to the earlier work by Dobrowolny et al. (1980) an initially asymmetric MHD turbulence $|z^+| \gg |z^-|$, like that observed close to the Sun by PSP (Chen et al. 2020), in absence of nonlinear interactions, should relax toward a state characterized by the presence of only one of the possible modes z^+ or z^-. Our main result is that the final state is not characterized by the absence of one of the two Alfvénic modes but that we are observing a different nature of the ***v–b*** coupling (Equations (11)–(12)), linked to the more/less Alfvénic nature of the solar wind close/far away from the Sun. This can also explain why close to the Sun an MHD Alfvénic turbulence as in Kraichnan is observed (Kraichnan 1965), with a spectral exponent $-3/2$, while close to the Earth a fluid turbulence scenario as in Kolmogorov (Kolmogorov 1941), with $\beta = -5/3$, can be drawn (Alberti et al. 2020; Chen et al. 2020). Our findings are also in agreement with models of balanced turbulence (Goldreich & Sridhar 1995; Schekochihin 2020),

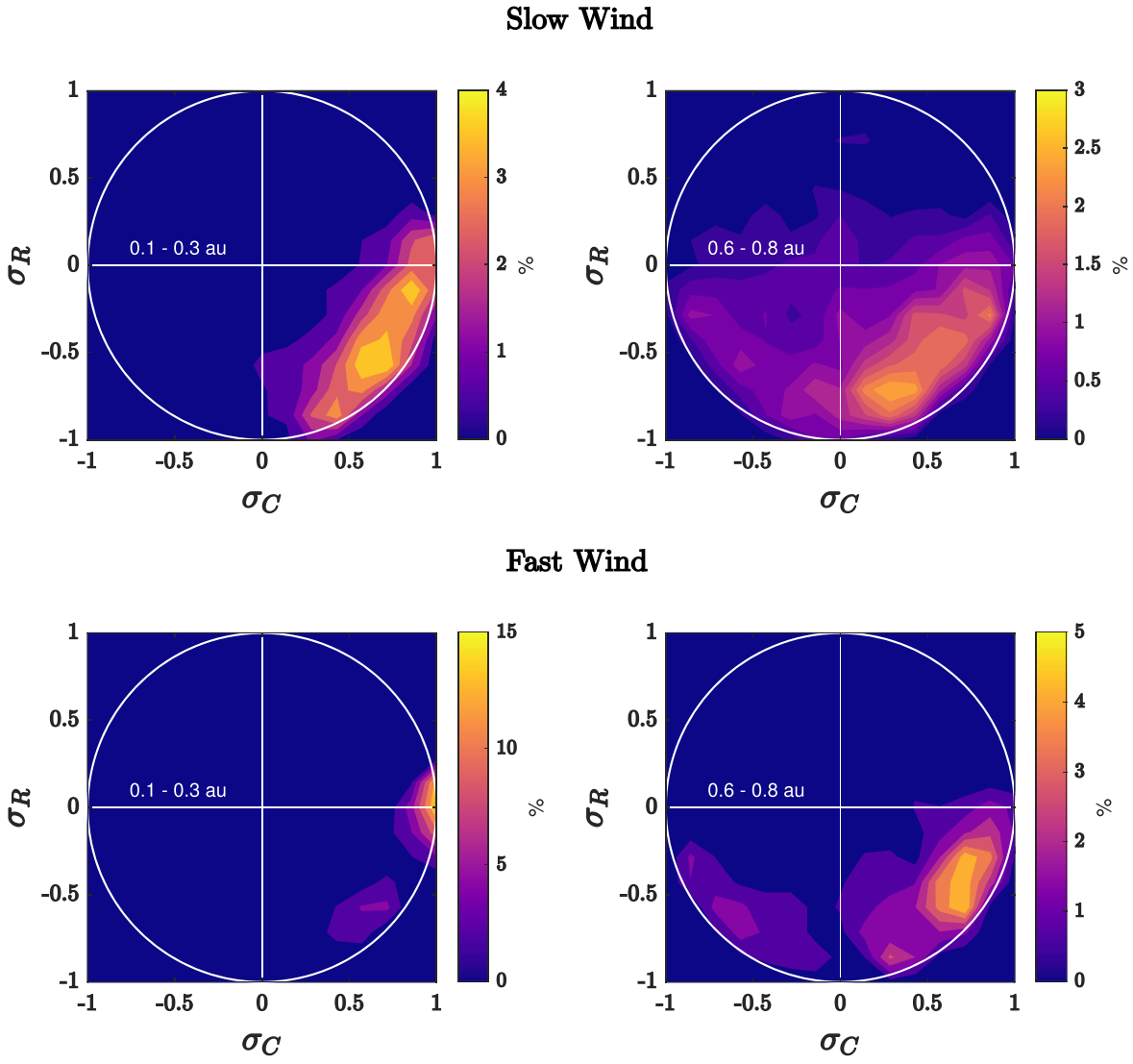

Figure 4. As in Figure 3 but separating slow ($V < 400$ km s^{-1}, upper panels) and fast ($V > 400$ km s^{-1}, lower panels) solar wind intervals.

suggesting that the observed changes in the spectral exponent can be related to a relaxation of the balanced turbulence scenario (Chen et al. 2020).

Since the *missing* element in the theoretical framework proposed by Dobrowolny et al. (1980) is the nonlinear term, we now discuss the fundamental implications of our results, in terms of the $\boldsymbol{v}$–$\boldsymbol{b}$ coupling, on the term $(z^{\mp} \cdot \nabla)z^{\pm}$, both for modeling approaches and for observational results. The nonlinear term (NL) can be written as

$$\mathrm{NL} = (z^{+} \cdot \nabla)z^{-} = [(\boldsymbol{v} + \boldsymbol{b}) \cdot \nabla](\boldsymbol{v} - \boldsymbol{b}), \tag{13}$$

which is

$$\mathrm{NL} = [(\boldsymbol{v} \cdot \nabla)\boldsymbol{v} - (\boldsymbol{b} \cdot \nabla)\boldsymbol{b}] + [(\boldsymbol{b} \cdot \nabla)\boldsymbol{v} - (\boldsymbol{v} \cdot \nabla)\boldsymbol{b}]. \tag{14}$$

The first term on the right-side of Equation (14) is the energetic part of the nonlinear term, i.e., it is related to the difference of the kinetic and the magnetic energy density. The second term on the right-side of Equation (14) is the mutual relation between $\boldsymbol{v}$ and $\boldsymbol{b}$. Indeed, due to the incompressible nature of Equations (1) the second term on the right-side of Equation (14) can be written as

$$[(\boldsymbol{b} \cdot \nabla)\boldsymbol{v} - (\boldsymbol{v} \cdot \nabla)\boldsymbol{b}] = \nabla \times (\boldsymbol{v} \times \boldsymbol{b}). \tag{15}$$

This allows us to revisit Equations (11)–(12) as

$$|z^{+}| \sim |z^{-}| \Rightarrow \boldsymbol{v} \cdot \boldsymbol{b} = 0 \Rightarrow \sigma_C = 0 \Rightarrow |\nabla \times (\boldsymbol{v} \times \boldsymbol{b})| \neq 0, \tag{16}$$

$$|z^{+}| \gg |z^{-}| \Rightarrow \boldsymbol{v} \cdot \boldsymbol{b} \gg 0 \Rightarrow \sigma_C = 1 \Rightarrow |\nabla \times (\boldsymbol{v} \times \boldsymbol{b})| \simeq 0. \tag{17}$$

Thus, moving away from the Sun an additional term appears in the nonlinear term that can be responsible for the observed radial behavior of some turbulence quantities, as σ_C but also the spectral/scaling properties, being related to the nature of the $\boldsymbol{v}$–$\boldsymbol{b}$ coupling. Thus, more efforts are needed to describe the evolution of the helical component of turbulence in the inner heliosphere that cannot be interpreted in a simple transport-like scenario but needs to be properly framed out in an evolving scenario, also involving the role of field coupling and intermittency (Schekochihin 2020).

Our results needs to be further assessed with more and more PSP orbits as well as with observations of the sub-Alfvénic

region that could open a completely different framework for the early stages of the solar wind turbulence evolution when leaving the Sun (Kasper et al. 2021). A critical view of the role of the turbulent cascade in the solar wind is needed, searching for novel models of the solar wind expansion that could be at the basis of the observed scenarios. Indeed, it has been recently demonstrated how including the expansion in solar wind modeling allows one to observe nearly equal spectral exponents for the Elsässer fields, as observed, also reproducing the observed variability of spectral indices at larger distances (Verdini et al. 2019; Grappin et al. 2021).

We acknowledge the NASA Parker Solar Probe Mission, the SWEAP team led by J. Kasper, and the FIELDS team led by S. D. Bale for use of data. The data can be downloaded from the NASA CDAWeb at https://cdaweb.gsfc.nasa.gov/pub/data/psp/. M.S. acknowledges the PhD course in Astronomy, Astrophysics and Space Science of the University of Rome "Sapienza," University of Rome "Tor Vergata" and Italian National Institute for Astrophysics (INAF), Italy. We particularly thank the anonymous reviewer for fruitful comments and suggestions that helped us to improve the significance and the clarity of our manuscript. G.C. acknowledges the financial support by Italian MIUR-PRIN grant 2017APKP7T on Circum-terrestrial Environment: Impact of Sun-Earth Interaction.

ORCID iDs

Tommaso Alberti https://orcid.org/0000-0001-6096-0220
Simone Benella https://orcid.org/0000-0002-7102-5032
Giuseppe Consolini https://orcid.org/0000-0002-3403-647X
Mirko Stumpo https://orcid.org/0000-0002-6303-5329
Roberto Benzi https://orcid.org/0000-0002-5335-7068

References

Adhikari, L., Zank, G. P., Bruno, R., et al. 2015, ApJ, 805, 63
Adhikari, L., Zank, G. P., & Zhao, L.-L. 2019, ApJ, 876, 26
Adhikari, L., Zank, G. P., Zhao, L.-L., & Telloni, D. 2022, ApJ, 933, 56
Adhikari, L., Zank, G. P., Zhao, L.-L., et al. 2020, ApJS, 246, 38
Alberti, T., Laurenza, M., Consolini, G., et al. 2020, ApJ, 902, 84
Alberti, T., Milillo, A., Heyner, D., et al. 2022, ApJ, 926, 174
Alberti, T., Narita, Y., Hadid, L. Z., et al. 2022, A&A, 664, L8
Allen, R. C., Lario, D., Odstrcil, D., et al. 2020, ApJS, 246, 36
Andrés, N., Sahraoui, F., Huang, S., Hadid, L. Z., & Galtier, S. 2022, A&A, 661, A116
Bale, S. D., Badman, S. T., Bonnell, J. W., et al. 2019, Natur, 576, 237
Bale, S. D., Goetz, K., Harvey, P. R., et al. 2016, SSRv, 204, 49
Bandyopadhyay, R., Matthaeus, W. H., McComas, D. J., et al. 2022, ApJL, 926, L1
Bavassano, B., Pietropaolo, E., & Bruno, R. 1998, JGR, 103, 6521
Bruno, R., D'Amicis, R., Bavassano, B., Carbone, V., & Sorriso-Valvo, L. 2007, AnGeo, 25, 1913
Chen, C. H. K., Bale, S. D., Bonnell, J. W., et al. 2020, ApJS, 246, 53
Chhiber, R., Goldstein, M. L., Maruca, B. A., et al. 2020, ApJS, 246, 31
Chhiber, R., Matthaeus, W. H., Bowen, T. A., & Bale, S. D. 2021, ApJL, 911, L7
Cuesta, M. E., Parashar, T. N., Chhiber, R., & Matthaeus, W. H. 2022, ApJS, 259, 23
D'Amicis, R., & Bruno, R. 2015, ApJ, 805, 84
Dobrowolny, M., Mangeney, A., & Veltri, P. 1980, PhRv, 45, 144
Dudok de Wit, T., Krasnoselskikh, V. V., Bale, S. D., et al. 2020, ApJS, 246, 39
Elsasser, W. M. 1950, PhRv, 79, 183
Fox, N. J., Velli, M. C., Bale, S. D., et al. 2016, SSRv, 204, 7
Goldreich, P., & Sridhar, S. 1995, ApJ, 438, 763
Grappin, R., Verdini, A., & Müller, W. C. 2021, in SF2A-2021: Proc. Annual Meeting of the French Society of Astronomy and Astrophysics, ed. A. Siebert et al. (Paris: Société Française d'Astronomie et d'Astrophysique), 222
Hellinger, P., Matteini, L., Landi, S., et al. 2015, ApJL, 811, L32
Kasper, J. C., Abiad, R., Austin, G., et al. 2016, SSRv, 204, 131
Kasper, J. C., Bale, S. D., Belcher, J. W., et al. 2019, Natur, 576, 228
Kasper, J. C., Klein, K. G., Lichko, E., et al. 2021, PhRvL, 127, 255101
Kolmogorov, A. 1941, DoSSR, 30, 301
Kraichnan, R. H. 1965, PhFl, 8, 1385
Lotekar, A., Vasko, I. Y., Phan, T., et al. 2022, ApJ, 929, 58
Malaspina, D. M., Halekas, J., Berčič, L., et al. 2020, ApJS, 246, 21
Matthaeus, W. H., & Goldstein, M. L. 1982, JGR, 87, 6011
Matthaeus, W. H., Oughton, S., Pontius, D. H. J., & Zhou, Y. 1994, JGR, 99, 19267
Oughton, S., Matthaeus, W. H., Wan, M., & Parashar, T. 2016, JGRA, 121, 5041
Parker, E. N. 1958, ApJ, 128, 664
Roberts, D. A., Klein, L. W., Goldstein, M. L., & Matthaeus, W. H. 1987, JGR, 92, 11021
Schekochihin, A. A. 2020, arXiv:2010.00699
Sioulas, N., Huang, Z., Shi, C., et al. 2022, arXiv:2209.02451
Stumpo, M., Quattrociocchi, V., Benella, S., Alberti, T., & Consolini, G. 2021, Atmos, 12, 321
Telloni, D., Sorriso-Valvo, L., Woodham, L. D., et al. 2021, ApJL, 912, L21
Verdini, A., Grappin, R., Montagud-Camps, V., et al. 2019, NCimC, 42, 17
Zank, G. P., Adhikari, L., Hunana, P., et al. 2017, ApJ, 835, 147
Zank, G. P., Adhikari, L., Hunana, P., et al. 2018, ApJ, 854, 32
Zank, G. P., Nakanotani, M., Zhao, L.-L., Adhikari, L., & Kasper, J. 2020, ApJ, 903, 1
Zank, G. P., Zhao, L.-L., Adhikari, L., et al. 2021, PhPl, 28, 080501
Zank, G. P., Zhao, L.-L., Adhikari, L., et al. 2022, ApJL, 926, L16